

T-STRESS SOLUTIONS FOR CRACKS IN STRAIGHT PIPES

R A Ainsworth¹, M Gintalas¹, K Abburi Venkata²

¹The University of Manchester, Pariser Building, Sackville Street, Manchester M13 9PL, UK.

²The University of Bristol, Queen's Building, University Walk, Bristol, BS8 1TR, UK

ABSTRACT

The increasing use of constraint arguments for defect assessments of large-scale components such as pipes requires estimates of suitable parameters to characterise crack tip constraint. The simplest such parameter is the elastic T-stress. However, for pipes, such solutions are not readily available. Therefore, this paper reports the results of an extensive series of finite element calculations to provide normalised T-stress solutions for pipes for a range of geometry and crack sizes. Comparisons with the limited solutions in the literature are used to give confidence in the numerical solutions obtained, which are shown to be sensitive to mesh refinement. The results are provided in a form that is suitable for use in practical defect assessments such as the constraint modified failure assessment diagram approach.

INTRODUCTION

Conventional single parameter fracture mechanics is complemented by a second parameter for more detailed assessment of cracked components. The stress intensity factor, K_I , may be paired with the elastic T-stress, for example. Two parameter approaches help to apply material fracture toughness from small-scale laboratory specimens to fracture in large-scale components. The K_I and T parameters are invoked when some constraint based failure assessment procedures are applied to cracked structural analysis. For example, a constraint-based fracture mechanics methodology based on a two-parameter K_I -T characterization of the crack tip fields could be successfully employed for constraint assessments in specimens and pipes (Dadfarnia et al (2011)).

T-stress solutions for two-dimensional geometries, including fracture mechanics specimens, are available in the literature or from compendia in failure assessment codes such as R6 (2015). However, T-stress solutions for 3D cracked bodies are still limited. The works by Huh (2006), Jayadevan et al (2005), Qian (2010) and Lewis and Wang (2008) address T-stress analysis in pipes with circumferential cracks. Only the work of Lewis and Wang (2008) deals with circumferential through-wall cracks in pipes.

This paper presents finite element studies for T-stress and stress intensity factor for circumferentially through-wall cracked pipes using three-dimensional elements. Results are compared with the solutions of Lewis and Wang (2008), which are based on analyses using shell elements.

T-STRESS

The stress intensity factor, K_I , measures the intensity of the elastic crack tip stress and strain fields and the T-stress characterizes the crack tip constraint. Positive T-stress increases the level of crack tip stress triaxiality and leads to high crack tip constraint. Negative T-stress reduces the level of crack tip stress triaxiality and leads to low crack tip constraint (Zhao and Guo (2012)). The T-stress is also capable of characterising constraint levels in 3D cracked bodies (Shlyannikov (2014)). As shown in Moustabchir et al (2012), the T-stress may be used to predict the potential propagation path of longitudinal and circumferential defects in pressure vessels. Moreover, analysis based on single edge notch tension and single edge notch bend specimens showed that the T-stress approach could be used not only to estimate initiation fracture toughness but also to develop constraint-corrected resistance curves (Zhou (2011)).

The elastic T-stress is directly proportional to the load applied to a cracked geometry and is the constant stress acting parallel to the crack flank in the near-tip elastic stress field:

$$\begin{Bmatrix} \sigma_{xx} \\ \sigma_{yy} \\ \tau_{xy} \end{Bmatrix} = \frac{K_I}{\sqrt{2\pi r}} \cos\left(\frac{\varphi}{2}\right) \begin{Bmatrix} 1 - \sin\left(\frac{\varphi}{2}\right) \sin\left(\frac{3\varphi}{2}\right) \\ 1 + \sin\left(\frac{\varphi}{2}\right) \sin\left(\frac{3\varphi}{2}\right) \\ \sin\left(\frac{\varphi}{2}\right) \cos\left(\frac{3\varphi}{2}\right) \end{Bmatrix} + \begin{Bmatrix} T \\ 0 \\ 0 \end{Bmatrix} \quad (1)$$

where $\sigma_{xx}, \sigma_{yy}, \tau_{xy}$ are the normal and shear stress components, K_I is the opening mode stress intensity factor, r is distance from the crack tip and φ is the polar angle (see Fig. 1). Then,

$$T = (\sigma_{xx} - \sigma_{yy})_{r \rightarrow 0, \varphi = 0} \quad (2)$$

When specimens with negative values of the T-stress are tested, there is an increase in the measured fracture toughness which is attributed to loss of constraint. The T-stress directly affects the hydrostatic stress. Negative values lower whereas positive values raise the hydrostatic stress. The T-stress may also influence the crack growth path. In general if $T < 0$, the crack propagation path follows a straight line and for $T > 0$ it follows a curve (Gupta, et al (2014), Sherry et al (1995) and Meliani et al (2010))

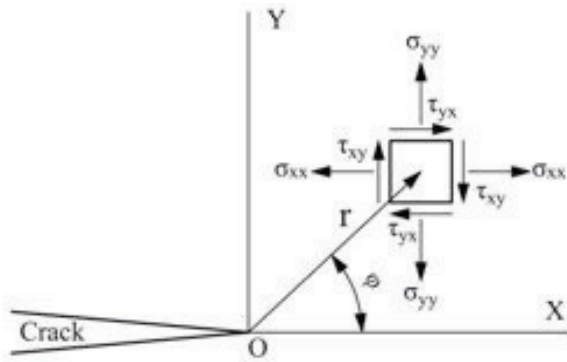


Figure 1. Stress state at the crack tip

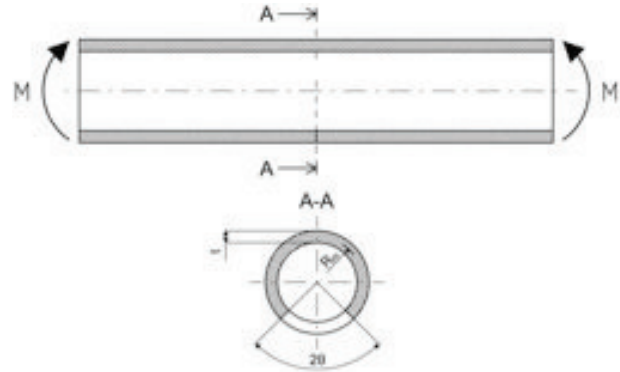


Figure 2. Pipe under pure bending moment M

The ratio of T-stress to the yield stress σ_y of the material is more important than the absolute value of T itself. Thus, in practical applications T is normalized by the yield stress of the material. The ratio T/σ_y is also directly proportional to the plastic collapse parameter L_r employed in the defect assessment procedure R6 (2015) and this is used to define a normalised constraint parameter β_T :

$$\beta_T L_r = T/\sigma_y \quad (3)$$

For the pipes analysed in this study (Figure 2), pure bending is considered for which the limit moment, M_L , is defined by:

$$M_L = 4R_m^2 t \sigma_y [\cos(0.5\theta) - 0.5 \sin \theta] \quad (4)$$

where R_m is the mean radius, t is the thickness and 2θ is the angle subtended by the crack (Figure 2).

ELASTIC FINITE ELEMENT MODEL OF CRACKED PIPE

The finite element (FE) study was performed to obtain T-stress and stress intensity factor values for the pipes being assessed using fitness-for-service approaches. These cases are addressed by sharp crack modelling in three-dimensional solids. The analyses are described below.

As the stress and strain gradients become large as a crack tip is approached, mesh refinement around the crack tip is required to capture stresses and strains accurately. For sharp crack modelling in a small-strain analysis the singularity at the crack tip should be considered. J-integral, stress intensity factors, and the stress and strain calculations are more accurate if the type of singularity is defined in the mesh at the region close to the crack tip. If r is the distance from the crack tip, the strain, ϵ , singularity in a small-strain elastic analysis is:

$$\epsilon \propto r^{-1/2} \quad (5)$$

This type of singularity is achieved by placing the first node away from the crack tip point at one-quarter of the distance to the second point. The crack tip was enclosed by the first contour of full integration wedge type C3D15 (9 integration points) elements. Midside nodes of the first contour elements were moved to the 0.25 points. The second contour and the remaining model were composed from full integration C3D20 (27 integration points) elements.

The accuracy of the results also depends on the angular resolution of the mesh around the crack tip. Stable and path independent results for the J-integral are obtained for LEFM if the crack tip is enclosed by elements, with two edges originating from the crack tip forming a minimum angle in the range from 10° to 22.5° (Figure 3). All models in this study had 16 elements around half of the crack tip. This results in an angle of 11.25° of single wedge element at the crack tip. A view of the mesh at the crack area is presented in Figure 3.

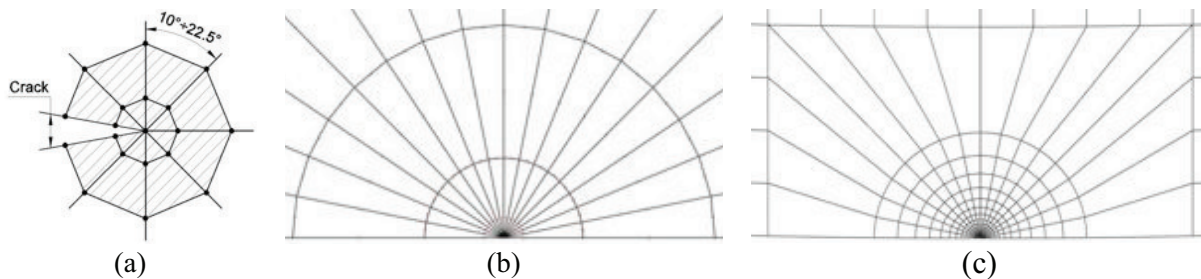


Figure 3. Mesh at the crack tip: (a) Recommended mesh type around crack tip for sharp crack analysis (b) Actual mesh: A view of 1st and 2nd contour around the crack tip (c) A view of the mesh at the crack tip area

The crack tip mesh zone in all models is represented by 1×2 mm rectangles (Figure 3c). The crack tip was enclosed by circular contours; the 20th contour had a radius of 0.5mm and contains the furthestmost nodes for extraction of results. The volume inside contains the remaining nineteen contours. The path independent T-stress and stress intensity factor values are obtained from values on contours from 3rd to

20th. However, path independence of the extracted values of T does not prove mesh convergence and therefore an independent mesh convergence study was performed.

The FE models were meshed with 11 elements through the thickness. Through the thickness, this gives 12 layers of nodes located on an element edge plane and 11 layers of nodes located on element mid-planes. In total, therefore, there are 23 layers of nodes through the thickness. Here, number 1, and hence R_1 , indicates the external surface and number 23 the inner surface, etc. Since T-stress estimation is inaccurate in regions close to where a crack intersects a free surface (Sherry et al (1995)), results from node layers numbered from 1 to 4 and from 20 to 23 were excluded from analysis. Thus results on node layers from 5 to 19 were considered and in ABAQUS, used in this study, the T-stress is extracted using an interaction integral technique.

In order to induce pure in-plane bending, rotation was applied to the end of a pipe using the MPC (multi-point constraint) constraint type option within ABAQUS. The end surface of the pipe was constrained by one master node located in the middle of the cross section. Then bending was applied to the master node. This constraint type allows rotation to be transferred from the master node via constrained slave surfaces to the pipe. The MPC option ensures that the rotated end surface remains straight during bending.

The mesh convergence study was performed for radius to thickness ratios $R_m/t=5, 10$ and 20 , by varying the element length along the pipe length, L (Figure 4). The length, L , was chosen as 100mm and the mean radius as $R_m=11\text{mm}$ for all analysed cases. The ratio, R_m/t , was varied by changing thickness, t . Around the semi-circumference of the cylinder, the mesh contained 34 elements resulting in an element size of $\text{edge} = 1\text{mm}$. This number of 34 elements around the semi-circumference was kept constant for all cases. Five steps of mesh refinement were performed for each value of R_m/t as presented in Table 1.

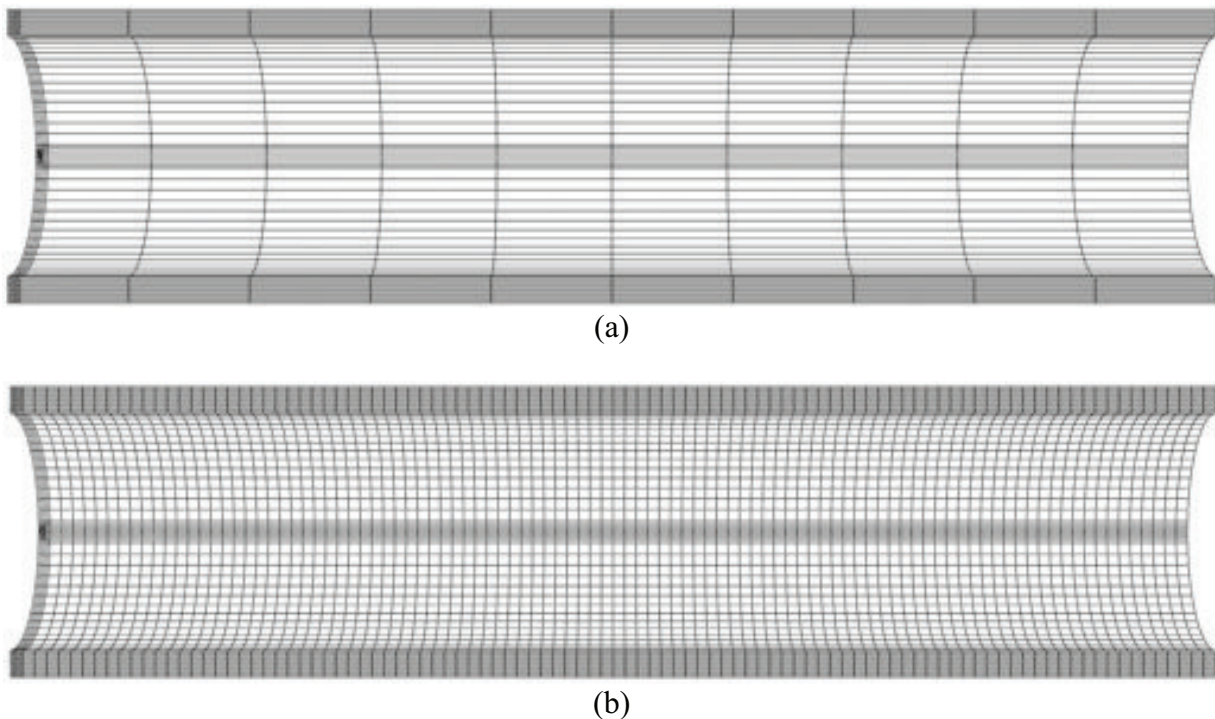


Figure 4. Model mesh of case $R_m/t=5, \theta/\pi=0.5$: (a) The coarsest mesh with 10 mm element length (b) The finest mesh with 1 mm element length

Table 1: Dimensions of pipes being simulated and the number of elements $N (\times 10^3)$ for each case

R_m/t	R_m [mm]	L [mm]	Element length in L direction				
	t [mm]		10 [mm]	5 [mm]	2.5	1.25[mm]	1 [mm]
5	11	100	10	14	23	38	48
	2.2						
10	11						
	1.1						
20	11						
	0.55						

FINITE ELEMENT STUDY RESULTS

Stress intensity factor

Results for the stress intensity factor from the mesh convergence study are shown in Figures 5-8. The figures contain values of the normalized stress intensity factor, F_b , at the mean radius, R_{12} , obtained from the FE study and a reference solution for $R_m/t=5, 10$ and 20 .

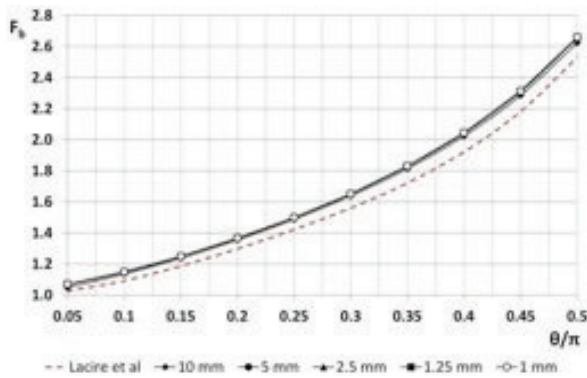


Figure 5. Normalized stress intensity factor F_b for $R_m/t=5$

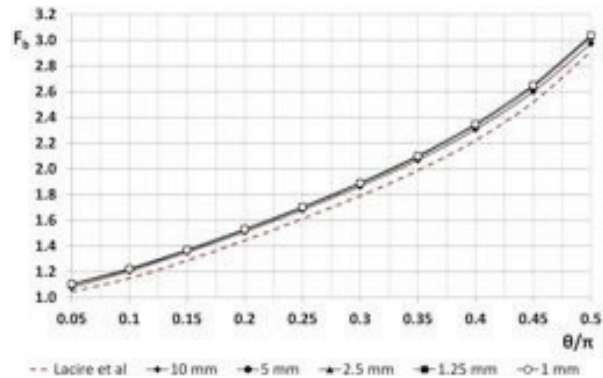


Figure 6. Normalized stress intensity factor F_b for $R_m/t=10$

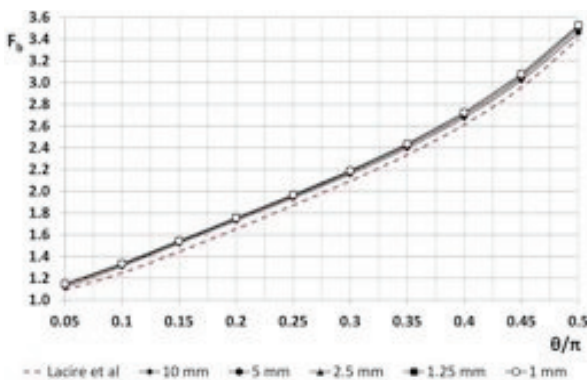


Figure 7 Normalized stress intensity factor F_b for $R_m/t=20$

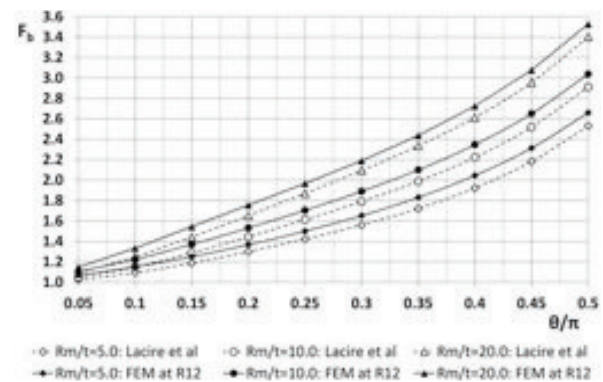


Figure 8. Normalized stress intensity factor F_b for $R_m/t=5, 10$ and 20 . 1 mm element size cases

The normalized stress intensity factor, F_b , of Lacire et al (1999) for circumferential through-wall cracked pipes was used as the reference solution:

$$F_b = \left[1 + (t/2R_m) \right] \left[A_b + B_b (\theta/\pi) + C_b (\theta/\pi)^2 + D_b (\theta/\pi)^3 + E_b (\theta/\pi)^4 \right]$$

$$\begin{aligned} A_b &= 0.65133 - 0.5774\eta - 0.3427\eta^2 - 0.0681\eta^3 & B_b &= 1.879 + 4.795\eta + 2.343\eta^2 - 0.6197\eta^3 \\ C_b &= -9.779 - 38.14\eta - 6.611\eta^2 + 3.972\eta^3 & D_b &= 34.56 + 129.9\eta + 50.55\eta^2 + 3.374\eta^3 \\ E_b &= -30.82 - 147.6\eta - 78.38\eta^2 - 15.54\eta^3 & \eta &= \log(t/R_m) \end{aligned} \quad (6)$$

The results indicate that higher values of R_m/t result in higher values of F_b , while an increase in crack angle θ results in higher values of F_b for all R_m/t . The stress intensity factor is not generally influenced by mesh density in this study, with results from the coarsest and finest meshes practically coincident with each other and with the reference solution.

T-stress

Results for the normalized T-stress from the mesh convergence study are shown in Figures 9 – 12. The T-stress from the current FE study of circumferential through-wall cracked pipes was compared with the solutions of Lewis and Wang (2008). There normalised T-stress solutions are given in the form:

$$T/\sigma_b = C_1 + C_2(\theta/\pi)^2 + C_3(\theta/\pi)^4 + C_4(\theta/\pi)^6 + C_5(\theta/\pi)^8 + C_6(\theta/\pi)^{10} \quad (7)$$

where the solutions are normalised by the bending stress $\sigma_b = M/(\pi R_m^2 t)$. The coefficients C_i ($i = 1 - 6$) in eqn (7) are functions of the radius to thickness ratio R_m/t :

$$C_i = C_{i0} + C_{i1}(R_m/t) + C_{i2}((R_m/t)^2) \quad (8)$$

where the coefficients C_{ij} are given in Table 2.

Table 2: Coefficients in eqn (8) from Lewis and Wang (2008)

i	Constraint Coefficient		
	C_{i0}	C_{i1}	C_{i2}
1	-0.934	-0.01	0.0005
2	4.3575	1.2671	-0.0451
3	74.273	-35.312	0.9889
4	-680.39	266.98	-6.3389
5	2688.6	-957.82	20.135
6	-3852.8	1325	-25.744

Figures 9-12 show values of normalized T-stress at the mean radius R_{12} obtained from the FE study and from Lewis and Wang (2008) for $R_m/t=5.0, 10.0, 20.0$.

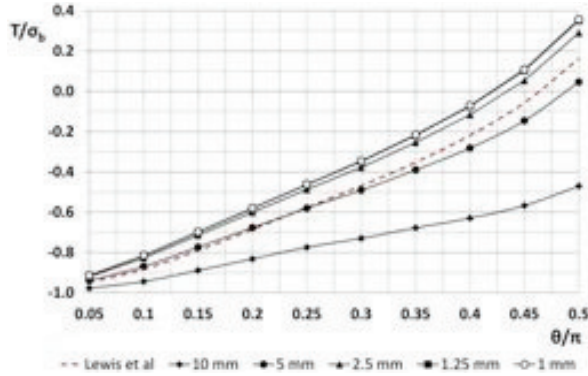


Figure 9. T/σ_b at mean radius for $R_m/t=5$

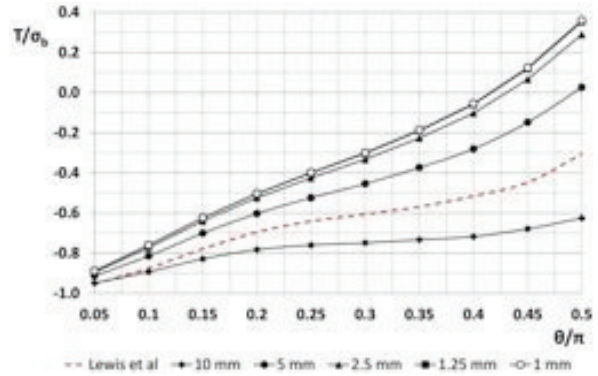


Figure 10. T/σ_b at mean radius for $R_m/t=10$



Figure 11. T/σ_b at mean radius for $R_m/t=20$

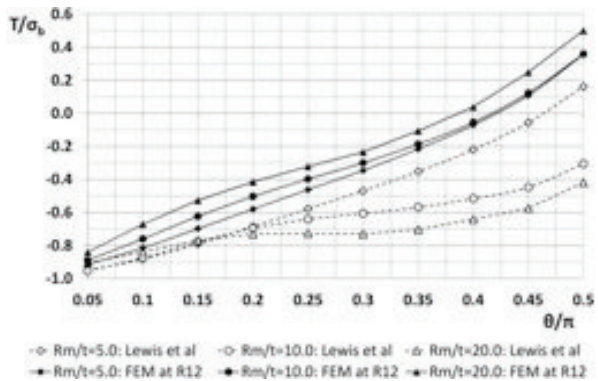


Figure 12. T/σ_b at mean radius for 1 mm element size

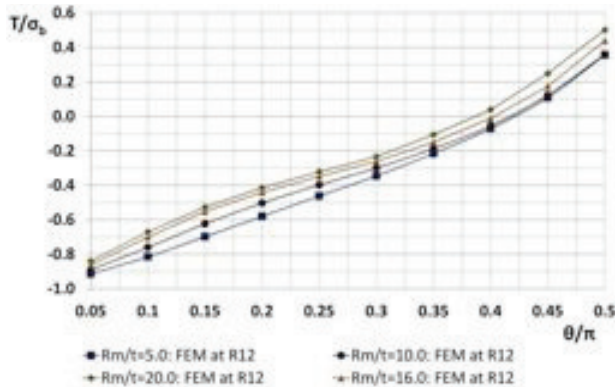


Figure 13. T/σ_b for $R_m/t=5, 10, 20$ and 16

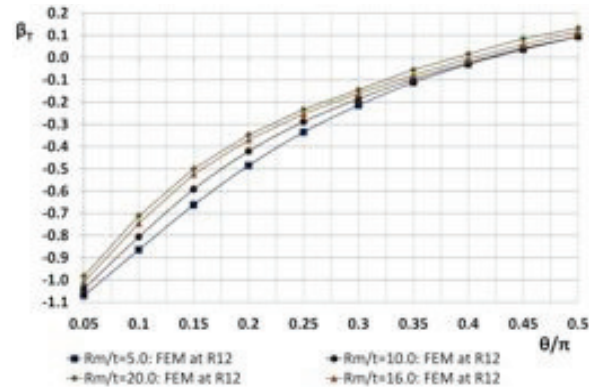


Figure 14. Constraint parameter β_T for $R_m/t=5, 10, 20$ and 16

Unlike the stress intensity factor, the T-stress estimate is sensitive to mesh density and this is discussed further below.

To provide information between $R_m/t = 10$ and 20 , an additional analysis was performed for $R_m/t=16.0$ and the results are included in Figure 13 for the converged solutions. Results from Figure 13 were

transformed into the normalised T-stress β_T using eqns (3) and (4) and are presented in Figure 14. A closed form solution was developed by applying curve fitting for each value of R_m/t leading to:

$$\beta_T = C_0 + C_1(\theta/\pi) + C_2(\theta/\pi)^2 + C_3(\theta/\pi)^3 + C_4(\theta/\pi)^4 + C_5(\theta/\pi)^5 + C_6(\theta/\pi)^6 \quad (9)$$

where the coefficients from C_0 to C_6 are given in Table 3.

Table: 3 Coefficients defining normalised constraint in equation (9)

R_m/t	C_6	C_5	C_4	C_6	C_6	C_6	C_0
5	296.15	- 558.19	426.24	- 163.76	27.617	2.1243	- 1.2269
10	477.76	- 917.07	686.29	- 244.65	35.891	2.4595	- 1.2267
16	940.06	- 1647.2	1107.5	- 345.34	41.751	3.3122	- 1.2423
20	576.85	- 1032.4	690.28	- 201.63	15.951	5.4587	- 1.2749

DISCUSSION

A key finding from this study is that the mesh refinement required to obtain converged T-stress solutions is much greater than that required to obtain converged stress intensity factor results. This is illustrated in Figures 15 and 16. It can be seen that the normalised stress intensity factor, Figure 15, shows little relative variation compared to that for T-stress, Figure 16. For selected cases, independent finite element analyses have been performed by the authors and a range of methods for evaluating T-stress have been used to give confidence in the results.

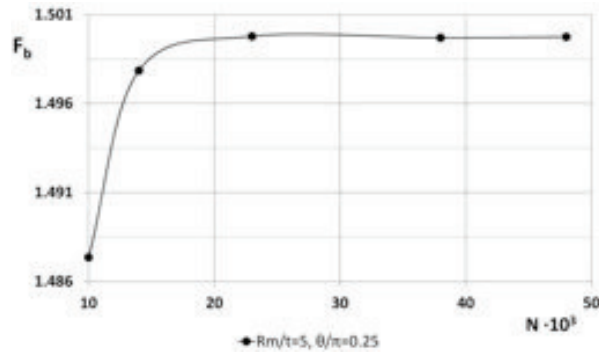


Figure 15. Normalised stress intensity factor, F_b , versus number of elements, N , in the model

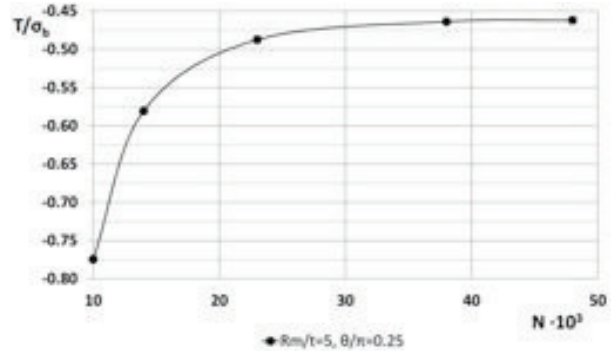


Figure 16. T/σ_b versus number of elements, N , in the model

Two possible reasons for the difference in convergence are as follows. First, an absolute error in stress near the crack tip, and hence in T-stress, leads to a reduced error in K_I by a factor proportional to $\sqrt{r/a}$, see equation (1). This would explain why convergence is better for smaller defect sizes, Figures 9-12. Secondly, it was found that the stresses σ_{xx} and σ_{yy} converged from above and below, respectively; therefore, the error in T-stress was essentially twice the error in either stress component, see equation (2) and Figure 17.

To examine this surprising result further, similar mesh refinement studies were performed using the same crack tip meshes for a single edge notched bend specimen with a crack depth equal to 20% of the section

thickness. The results of the convergence studies are shown in Figure 18, in terms of the normalised T-stress of equation (3), and show similar trends to those obtained for the more complex cylinder geometry. Further, the 3-D converged solution is within 10% of the handbook plane strain 2-D solution (R6, 2015) for the bend specimen, giving additional confidence in the accuracy of the converged solutions.

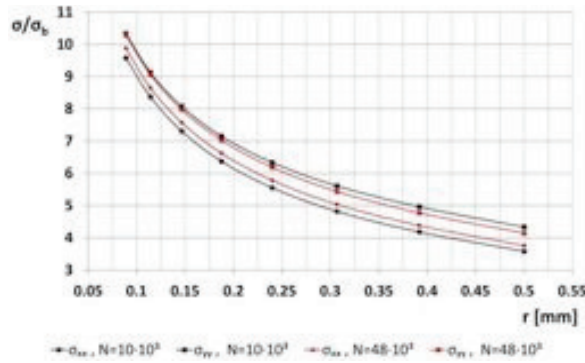


Figure 17. Distribution of σ_{xx} and σ_{yy} at the position $\varphi=0^\circ$ for the case $R_m/t=5$, $\theta/\pi=0.25$

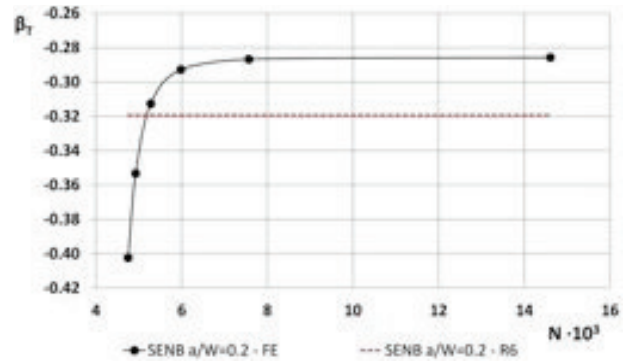


Figure 18. Mesh convergence in terms of β_T in SENB specimen

Overall, therefore it appears that caution should be exercised in the use of T-stress solutions in the literature, where mesh refinement studies have been limited to demonstration of acceptable stress intensity factor solutions.

CONCLUSIONS

The finite element study of circumferentially through-wall cracked pipes under in plane bending, reported in this paper, indicates that the results for stress intensity factor are much less sensitive to element size than those for T-stress. Therefore, highly refined meshes have been used here to develop T-stress solutions for a range of crack sizes and pipe radius to thickness ratio. The solutions have been fitted by a polynomial with coefficients defined for a range of radius to thickness ratios, and thus are in a form suitable for use in practical fitness-for-service assessment approaches.

ACKNOWLEDGEMENTS

Support from the Engineering and Physical Sciences Research Council (EPSRC) under grant reference EP/K007815/1 is gratefully acknowledged.

REFERENCES

- Dadfarnia, M., Sofronis, P., Somerday, B. P., Balch, D. K., Schembri, P., and Melcher, R. (2011). "On the environmental similitude for fracture in the SENT specimen and a cracked hydrogen gas pipeline," *Engng Fract Mech* 78, 2429-2438.
- Gupta, M., et al, (2014). "A review of T-stress and its effects in fracture mechanics," *Engng Fract Mech*, <http://dx.doi.org/10.1016/j.engfracmech.2014.10.013>
- Huh, N-S (2006). "Elastic T stress estimates for circumferential surface-cracked cylinders," *Fatigue Fract Engng Mater Struct* 29, 57-59.
- Jayadevan, K. R., Thaulow, C., Ostby, E., Berg, E., Skallerud, B., Holthe, K., and Nyhus, B (2005). "Structural integrity of pipelines: T-stress by line-spring," *Fatigue Fract Engng Mater Struct* 28, 467-88.

- Lacire, M. H., Chapuliot, S. and Marie, S. (1999). "Stress intensity factors of through wall cracks in plates and tubes with circumferential cracks," *ASME PVP* 388, 13–21.
- Lewis, T. and Wang, X. (2008). "The T-stress solutions for through-wall circumferential cracks in cylinders subjected to general loading conditions," *Engng Fract Mech* 75, 3206-3225.
- Meliani, M. H., Azari, Z., Pluvinage, G. and Matvienko, Y. G. (2010). "The effective T-stress estimation and cracks emanating from U-notches," *Engng Fract Mech* 77, 1682-1692.
- Moustabchir, H., Azari, Z., Hariri, S., and Dmytrakh, I. (2012) "Experimental and computed stress distribution ahead of a notch in a pressure vessel: Application of T-stress conception," *Comp Mater Sci* 58, 59-66.
- Qian, X. (2010). "K_I-T estimation for embedded flaws in pipes-Part II: Circumferentially oriented cracks," *Int J Pres Ves Piping* 87, 150-164.
- R6: Assessment of the integrity of structures containing defects, Revision 4, including subsequent updates (2015). EDF Energy Generation, Gloucester, UK.
- Sherry, A. H., France, C. C. and Goldthorpe, M. R. (1995). "Compendium of T-stress solutions for two and three dimensional cracked geometries," *Fatigue Fract Engng Mater Struct* 18(1),141-155.
- Shlyannikov, VN., et al (2014). "The elastic and plastic constraint parameters for three-dimensional problems," *Engng Fract Mech*, <http://dx.doi.org/10.1016/j.engfracmech.2014.05.015>
- Zhao, J. and Guo, W. (2012). "Three-parameter K-T-T_z characterization of the crack-tip field in compact-tension-shear specimens," *Engng Fract Mech* 92, 72-88.
- Zhou, D. W. (2011). "Measurement and modelling of R-curves for low constraint specimens," *Engng Fract Mech* 78, 605-622.